

# MGRR-Net: Multi-level Graph Relational Reasoning Network for Facial Action Units Detection

Xuri Ge, Joemon M. Jose, Songpei Xu, Xiao Liu, Hu Han, *Member, IEEE*,

**Abstract**—The Facial Action Coding System (FACS) encodes the action units (AUs) in facial images, which has attracted extensive research attention due to its wide use in facial expression analysis. Many methods that perform well on automatic facial action unit (AU) detection primarily focus on modeling various types of AU relations between corresponding local muscle areas, or simply mining global attention-aware facial features, however, neglect the dynamic interactions among local-global features. We argue that encoding AU features just from one perspective may not capture the rich contextual information between regional and global face features, as well as the detailed variability across AUs, because of the diversity in expression and individual characteristics. In this paper, we propose a novel Multi-level Graph Relational Reasoning Network (termed *MGRR-Net*) for facial AU detection. Each layer of MGRR-Net performs a multi-level (*i.e.*, region-level, pixel-wise and channel-wise level) feature learning. While the region-level feature learning from local face patches features via graph neural network can encode the correlation across different AUs, the pixel-wise and channel-wise feature learning via graph attention network can enhance discrimination ability of AU features from global face features. The fused features from the three levels lead to improved AU discriminative ability. Extensive experiments on DISFA and BP4D AU datasets show that the proposed approach achieves superior performance than the state-of-the-art methods.

**Index Terms**—Facial action units, multi-branch, graph neural network, multi-level, local-global interaction, multi-head graph attention network

## I. INTRODUCTION

Facial action units (AUs) are defined as a set of facial muscle movements that correspond to a displayed expression according to Facial Action Coding System (FACS) [1]. As a fundamental research problem, AU detection is beneficial to facial expression analysis [2], [3], and has wide potential applications in diagnosing mental health issues [4], improving e-learning experiences [5], detecting deception [6], *etc.* However, AU detection is challenging because of the difficulty in identifying the subtle facial changes caused by AUs, as well

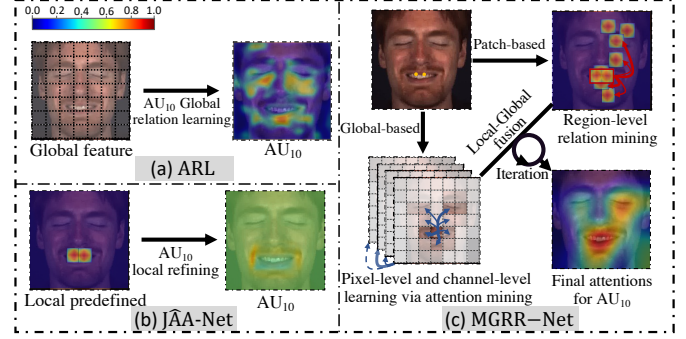


Fig. 1. Comparisons between the proposed method and two state-of-the-art methods in AU feature learning, and the corresponding visualized activation maps for AU10 (Upper Lip Raiser / Levator labii superioris). (a) ARL [9] performs global feature learning, (b) JAA-Net [10] learns from predefined local regions based on the landmarks, and (c) multi-level feature learning from both local regions and global face.

as due to individual physiology. Some earlier studies [7], [8] design hand-crafted features to represent the appearance of different local facial regions, according to the corresponding movements of facial muscles. However, hand-crafted shallow features are not discriminative enough to represent the rich facial morphology. Hence, deep learning based AU detection methods that rely on global and local facial features have been studied to enhance the feature representation of each AU.

Several recent works [11], [9], [12] aim to enhance the corresponding AU feature representation by combining the affected features in a deep global face feature map. For instance, LP-Net [12] using an LSTM model [13] combines the patch features from grids of equal partition made by a global Convolutional Neural Network (CNN). ARL [9] directly learns spatial attentions from the global CNN features of independent AU branches, as shown in the upper left of Fig. 1. However, these methods failed to focus on the right muscle area corresponding to each AU, which is often affected by some irrelevant regions. In the past, issues like these are addressed by methods [14], [15], [10] extracting AU-related features from regions of interest (ROIs) centered around the associated facial landmarks, which provide more precise muscle locations for AUs and lead to a better AU detection performance. For example, JAA [15] and JAA-Net [10] propose attention-based deep models to adaptively select the highly-contributing neighboring pixels of initially predefined muscle region for joint AU detection and face alignment, as shown in the lower left of Fig. 1. However, the above local attention-based

Xuri Ge is with the School of Computing Science, University of Glasgow, Scotland, UK (e-mail: x.ge.2@research.gla.ac.uk).

Joemon M. Jose is with the School of Computing Science, University of Glasgow, Scotland, UK (e-mail: joemon.jose@glasgow.ac.uk).

Songpei Xu is with the School of Computing Science, University of Glasgow, Scotland, UK (e-mail: s.xu.1@research.gla.ac.uk).

Xiao Liu is with the Online Media Business Unit at Tencent, Beijing 100080, China (e-mail: ender.liux@gmail.com).

Hu Han is with the Key Laboratory of Intelligent Information Processing, Institute of Computing Technology, Chinese Academy of Sciences, Beijing 100190, China, and also with Peng Cheng Laboratory, Shenzhen 518055, China (e-mail: hanhu@ict.ac.cn).

methods emphasize learning the appearance representation of each facial region based on detected landmarks, while ignoring some intrinsic dependencies between different facial muscles. For example, AU2 (“Outer Brow Raiser”) and AU7 (“Lid Tightener”) will be activated simultaneously when scaring. To this end, there exist several methods [16], [17], [18] that utilizing prior knowledge of AU correlation to define a fixed graph to exploit useful information from correlated AUs. It is difficult to capture effectively the dynamic relationships between AUs and the distinction of related AUs by a single predefined graph with a statistical prior from all faces, due to the variety of expressions and individual characteristics. Recent works [19] utilize an adaptive graph to model the relationship between AUs based on the global face, however, ignores the distinctive modeling of the local and global details of each AUs.

In this paper, we argue that the fundamental issues of facial AU detection lie in modeling the flexible relationships between corresponding muscle regions and improving the discrimination power of each AUs. On one hand, region-level dynamic AU relevance mining based on the detected landmarks accurately detect the corresponding muscles and flexibly model the relevance among muscle regions. It is different from the existing methods focusing on single AU region [15], [10] or a predefined fixed graph, with prior knowledge, for all faces [20]. On the other hand, learning the sensitivity of the target AU within the global face can better capture and accurately interpret and distinguish among different AUs. To the best of our knowledge, this idea is left unexploited in existing works [18], [20], [10].

Motivated by the above insights, we propose a novel technique for facial AU detection called MGRR-Net. Our main innovations lie in three aspects, as shown in the right of Fig. 1. Firstly, we introduce a dynamic graph to model and reason the relationship between a target AU and other AUs. The region-level AU features (as nodes) can accurately locate the corresponding muscles. Secondly, we supplement each AU with different levels (channel and pixel-level) of attention-aware details from global features, which greatly improves the distinction between AUs. Finally, we iteratively refine the AU features of the proposed multi-level local-global relational reasoning layer, which makes them more robust and more interpretable. In particular, we extract the global features by multi-layer CNNs and precise AU region features based on the detected facial landmarks, which serve as the inputs of each multi-level relational reasoning layer. A region-level AU graph is constructed to represent the relationships by the adjacency matrix (as edges) among AU regions (as nodes), initialized by prior knowledge and iteratively updated. We propose a method to learn channel-wise and pixel-wise semantic relations for different AUs at the same time by processing them in two separate efficient and effective multi-head graph attention networks (MH-GATs) [21]. Through this, we model the complementary Channel and pixel-level global details. After these local and global relation-oriented modules, a hierarchical gated fusion strategy helps to select more useful information for the final AU representation in terms of different individuals.

The contributions of this work are as follows:

- We propose a novel end-to-end iterative reasoning and training scheme for facial AU detection, which leverages the complementary multi-level local-global relations to improve robustness and discrimination for AU detection;
- We construct a region-level AU graph with the prior knowledge initialization and dynamically reason the correlated relationship of individual AUs, thereby improving the robustness of AU detection;
- We propose a GAT-based model to improve the discrimination of each local AU patch by supplementing multiple levels of global features;
- The proposed MGRR-Net outperforms the state-of-the-art approaches for AU detection on two widely used benchmarks, *i.e.*, BP4D and DISFA, without any external data or pre-trained models.

## II. RELATED WORK

1) *Facial AU detection.*: Most existing approaches for facial AU detection use feature learning from local patches [22], [14], [23], [15], [24], [12], [10]. However, in some early works [25], [26] there is a need to pre-define the patch location first. For instance, [27] proposed to use domain knowledge and facial geometry to pre-select a relevant image region (as patch) for a particular AU and feed it to a convolutional and bi-directional Long Short-Term Memory (LSTM) [28] neural network. [22] proposed a set of adaptive ROI cropping nets, based on local convolutional neural network, to learn regional features separately. [15] proposed an end-to-end deep learning framework for joint AU detection and face alignment, which used the detected landmarks to locate specific AU regions. However, all the above methods focused only on independent regions, without considering the correlations among different AU areas to reinforce and diversify each other. Recent works pay attention to capture the relations among AUs for local feature enhancement, which can improve robustness compared to using single patch features or global face. [20] incorporated AU knowledge-graph as an extra guidance for the enhancement of facial region representation. [18] applied the spectral perspective of graph convolutional network (GCN) for AU relation modeling, which also needed an additional AU correlation reference extracted from EAC-Net [29]. However, these methods need the prior knowledge by co-occurrence probability in different datasets to construct the fixed relation matrix instead of dynamically update for different expressions and individuals. [30] proposed a complex skip-BiLSTM to mine the potential mutual assistance and exclusion relationship between AU branches and simple global information complement. [31] proposed a performance-driven Monte Carlo Markov Chain to generate graphs from global face, which also capture some irrelevant regions. Moreover, these approaches usually ignored or simply fused the local and global information for each AU without considering the importance (important and non-important) of features.

2) *Graph Neural Network.*: Recently, integrating graphs with deep neural networks is an emerging topic in deep learning research. GCNs have been widely used in many

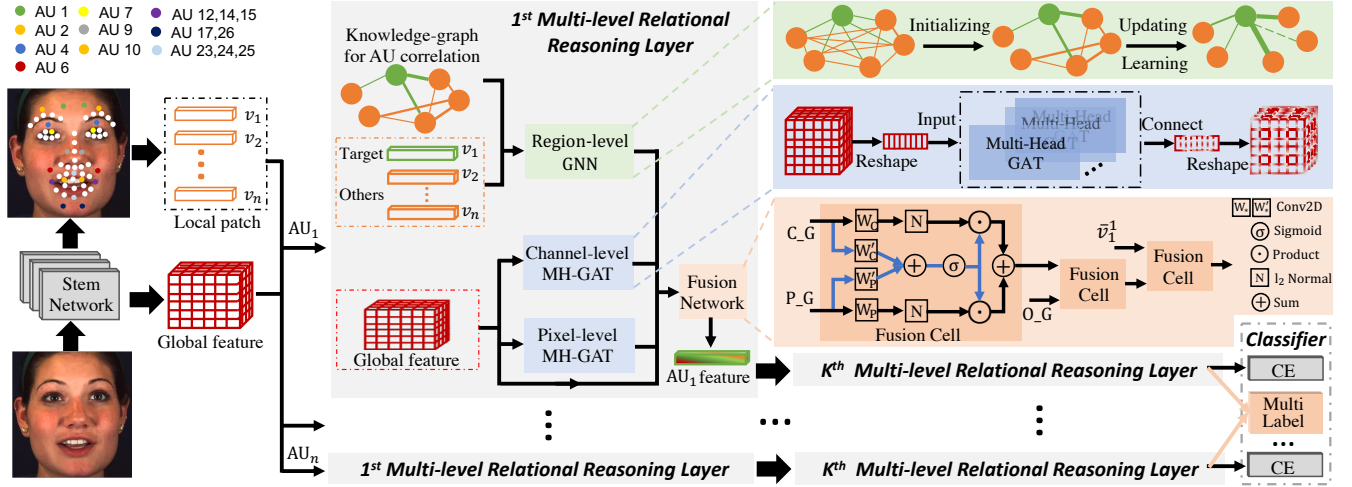


Fig. 2. The overall architecture of the proposed MGRR-Net for facial AU detection. Given one face image, the region-level features of local AU patches are extracted based on the detected landmarks from an efficient landmark localization network. The original global feature is extracted from the same shared stem network. Then the region-level GNN initialized with prior knowledge is applied to encode the correlation between different AU patches. Two separate MH-GATs are adopted to get two levels of global attention-aware features to supplement each AU. Finally, multiple levels of local-global features are fused by a hierarchical gated fusion strategy and refined by multiple iterations (best viewed in color).

application such as human action recognition [32], social relationship understanding [33] and object parsing [34]. [20] proposed to apply gated graph neural network (GGNN) with the guidance of AU knowledge-graph on facial AU detection. [17] embedded the relations among AUs through a predefined GCN to enhance the local semantic representation. However, these AU detection methods require a fixed predefined graph from different datasets when applying GGNN or GCN. [31], [19] applied an adaptive graph to model the relationships between AUs based on global feature, ignoring local-global interactions. Recently, a novel graph attention network with multi-head (MH-GAT) leverages masked self-attentional layers to operate on graph-structured data, which shows high computational efficiency.

In this paper, we argue that the relevance and diversity among AUs change dynamically due to diversities in expression and individual characteristics. In contrast to previous studies, our proposed MGRR-Net automatically models the relevance among the facial AU regions by a dynamic matrix as a graph and supplements each AU patch with multiple levels of global features to improve the variability. Multiple layers of iterative refinement greatly improve the AU discrimination ability.

### III. APPROACH

As shown in Fig. 2, the proposed approach consists of two key modules in each relational reasoning layer, *i.e.*, region-level local feature learning with relational modeling, and global feature learning with channel-level and pixel-level attention. A hierarchical gated fusion network is designed to combine multi-level local and global features as the new target AU feature. Finally, after multiple layers of iterative refinement and updating, the AU features are fed into a multi-branch classification network for AU detection. For clarity, the main notations and their definitions throughout the paper are shown in Table I.

#### A. Global and Local Features Extraction

Given a face image  $I$ , we adapt a stem network from the widely used multi-branch network [15] to extract the original global feature  $O\_G$  and further obtain the AU regions based on the detected landmarks. The stem network is shared by all branches to reduce training costs and the complexity of network training. In particular, a hierarchical and multi-scale region learning module in the stem network extracts features from each local patch with different scales, thus obtaining multi-scale representations. A series of landmarks  $S = \{s_1, s_2, \dots, s_m\}$  with length  $m$  are detected by an efficient face alignment module similar to [10], including three convolutional blocks connected to a max-pooling layer. According to the detected landmarks, local patches are calculated and their features  $V = \{v_1, v_2, \dots, v_n\}$  are learned via the stem network, where  $n$  is the number of selected AU patches. For simplicity, we do not repeat the detailed structure of the stem network here.

#### B. Multi-level Relational Reasoning Layer

After we get the original global feature  $O\_G$  for a face and the local region features  $V = \{v_1, v_2, \dots, v_n\}$  for AUs, a multi-layer multi-level relational reasoning model is introduced to automatically explore the relationship of individual local facial regions and supply two levels of global information. Fig. 2 shows the detailed structure of the 1<sup>st</sup> multi-level relational reasoning layer.

1) *Region-level Local Feature Relational Modeling.*: Different from the predefined fixed AU relationship graph in [20], we construct a fully-connected graph  $D\_G$  for all AUs, where the region-level features constitute the nodes, and a learnable adjacency matrix  $A$  constitutes the edges at each layer to represent the potential for co-occurrence of AUs (co-activated or non-activated). The AU relationships that have no co-occurrence or low co-occurrence in the training set will not be completely neglected either in comparison with [20], [17],

TABLE I  
MAIN NOTATIONS AND THEIR DEFINITIONS.

| Notation                 | Definition  |
|--------------------------|---|
| $I$                      | a facial image  |
| $S$                      | a set of detected landmarks                                   |
| $O\_G$                   | the original global feature                                   |
| $m$                      | the number of detected landmarks                              |
| $V$                      | a set of calculated patch features                            |
| $v_i$                    | the feature of $i$ -th patch                                  |
| $n$                      | the number of calculated patches corresponding to AUs         |
| $D\_G$                   | a fully-connected graph                                       |
| $A$                      | a learnable adjacency matrix                                  |
| $a_i$                    | the activation status of the $i$ -th AU                       |
| $P_{ij}$                 | the coefficient between $i$ -th and $j$ -th AU                |
| $P, C$                   | a set of pixel- and channel-level features                    |
| $P\_G$                   | the pixel-level attention-aware global feature                |
| $C\_G$                   | the channel-level attention-aware global feature              |
| $L$                      | the number of parallel attention layers                       |
| $K$                      | the number of relational reasoning layers                     |
| $\bar{v}_i^k$            | the feature of $i$ -th AU patch after $k$ -th reasoning layer |
| GFC                      | a gated fusion cell   |
| $(x_i, y_i)$             | the ground-truth coordinate of the $i$ -th facial landmark    |
| $(\hat{x}_i, \hat{y}_i)$ | the predicted coordinate of the $i$ -th facial landmark       |
| $d_o$                    | the ground-truth inter-ocular distance                        |
| $p_i$                    | the ground-truth occurrence probability of $i$ -th AU         |
| $\hat{p}_i$              | the predicted occurrence probability of $i$ -th AU            |

[18]. During the training process, we utilize prior knowledge to initialize  $A$  to assist and constrain learning. Specifically, the dynamic graph  $D\_G$  is composed of nodes (the local region features  $V = \{v_1, v_2, \dots, v_n\}$ ) and edges (the relationship matrix  $A$  among AUs). Following [17], we calculate the relationship coefficients between AUs from datasets as the initialization of the adjacency matrix  $A$ . The relationship coefficient  $A_{ij}$  of  $i$ -th and  $j$ -th AU can be formulated as:

$$P_{ij} = \frac{1}{2}(P(a_i = 1|a_j = 1) + P(a_i = 0|a_j = 0)), \quad (1)$$

$$A_{ij} = |(P_{ij} - 0.5) * 2| \quad (2)$$

where  $a_i=1$  denotes  $i$ -th AU is activated and 0 otherwise,  $|\cdot|$  means absolute value function. From Eq.1 and Eq.2,  $P(a_i=1|a_j=1)=0.5$  means that when  $j$ -th AU is activated, the probability of occurrence is equal to the no occurrence for  $i$ -th AU. It indicates that the activation of  $j$ -th AU could not provide useful information for the  $i$ -th AU and therefore no edge is connected.

2) *Attention-aware Global Features Learning.*: We argue that complementary global feature can improve the discrimination between AUs, which also alleviates the over-smoothing issue in graph neural networks for local relationship modeling. To this end, we employ two separate high-efficiency GAT models [21] to perform channel and pixel-level attention-aware global features from original deep visual features in order to handle expression and subject diversities. Specifically, we reshape the original global feature  $O\_G \in \mathbb{R}^{(c,w,h)}$  into a set of channel-level features  $\{C_1, \dots, C_c\}$ ,  $C_i \in \mathbb{R}^{w*h}$ . Similarly, we

get a set of pixel-level features  $\{P_1, \dots, P_{w'*h'}\}$ ,  $P_i \in \mathbb{R}^c$ , from  $O\_G$  after a convolution in order to reduce the parameters. The attention coefficients for each level of features are calculated in GAT, which can be formulated as:

$$\alpha_{ij} = \frac{\exp(U_q C_i (U_k C_j)^T / \sqrt{D})}{\sum_{o \in \Omega_i} \exp(U_q C_i (U_o C_o)^T / \sqrt{D})}, \quad (3)$$

where  $U_q, U_k, U_o$  are the parameters of mapping from  $w * h$  to  $D$  and  $\Omega_i$  denotes neighborhoods of  $C_i$ .  $\sqrt{D}$  acts as a normalization factor. Following [35], [21], we also employ multi-head dot product by  $L$  parallel attention layers to speed up the calculation efficiency. The overall working flow is formulated as:

$$\bar{C}_i = \text{ReLU}(\sum_{o \in \Omega_i} U_c ||U'_q C_i (U'_k C_o)^T / \sqrt{d}||), \quad (4)$$

$$\alpha_{ij}^l = \frac{\exp(U'_q C_i (U'_k C_j)^T / \sqrt{d})}{\sum_{o \in \Omega_i} \exp(U'_q C_i (U'_o C_o)^T / \sqrt{d})}, \quad (5)$$

where  $U_c$  is the mapping parameter,  $U'_q, U'_k, U'_o$  map the feature dimension to  $1/L$  of the original,  $||$  means concatenation, and  $d$  equals  $D/L$ . Finally, new channel-level attention-aware global feature  $C\_G$  is reshaped to the same domination with  $O\_G$ . With the same process on pixel-level features  $\{P_1, \dots, P_{w'*h'}\}$ , we can get the final pixel-level attention-aware global features  $P\_G$  after a deconvolution layer behind of a GAT with multi-head (MH-GAT).

3) *Hierarchical Fusion and Iteration.*: We iteratively refine the  $i$ -th target AU feature of the proposed multi-level relational reasoning layer  $K$  times, which obtains other correlated local regional information and provides rich global information in each layer. The process can be formulated as:

$$\bar{v}_i^k = W_i^k v_i^k + \sum_j^n (A_{ij}^k W_j^k v_j^k), \quad (6)$$

where  $W^k$  is the mapping parameter and  $A_{ij}^k$  means the learnable correlation coefficient between  $AU_i$  and  $AU_j$  at  $k$ -th layer. We then use a hierarchical fusion strategy by a gated fusion cell (GFC) to complement the global multi-level information for each updated AU feature at  $k$ -th layer as follows:

$$\bar{v}_i^{k+1} = \text{GFC}(\bar{v}_i^k, \text{GFC}(O\_G^k, \text{GFC}(C\_G^k, P\_G^k))), \quad (7)$$

We define the operation of GFC as follows:

$$\begin{aligned} & \text{GFC}(C\_G^k, P\_G^k) \\ &= \beta \odot \|W_C^k C\_G^k\|_2 + (1 - \beta) \odot \|W_P^k P\_G^k\|_2, \end{aligned} \quad (8)$$

$$\beta = \sigma(W_C^{k'} C\_G^k + W_P^{k'} P\_G^k), \quad (9)$$

where  $\sigma$  is the sigmoid function, and  $\|\cdot\|$  denotes the  $l_2$ -normalization.  $W_C^k$  and  $W_P^k$  denote the Conv2D operation.

### C. Joint Learning

A multi-label binary classifier is used to classify the AU activation state, which adopt a weighted multi-label cross entropy loss function as follows,

$$\mathcal{L}_{au} = -\frac{1}{n} \sum_{i=1}^n w_i [p_i \log \hat{p}_i + (1 - p_i) \log (1 - \hat{p}_i)], \quad (10)$$

TABLE II  
COMPARISONS OF AU RECOGNITION FOR 8 AUs ON DISFA IN TERMS OF F1-FRAME SCORE (IN %). \* MEANS THE METHOD EMPLOYED PRETRAINED MODEL ON ADDITIONAL DATASET, SUCH AS IMAGENET AND VGGFACE2, *etc.*

| Method                                  | AU Index    |               |               |               |               |             |               |               | Avg.          |
|---|-------------|---------------|---------------|---------------|---------------|-------------|---------------|---------------|---------------|
|   | 1           | 2             | 4             | 6             | 9             | 12          | 25            | 26            |               |
| Without additional augmented data       |             |               |               |               |               |             |               |               |               |
| DSIN [36]                               | 42.4        | 39.0          | 68.4          | 28.6          | 46.8          | 70.8        | 90.4          | 42.2          | 53.6          |
| JAA [15]                                | 43.7        | 46.2          | 56.0          | 41.4          | 44.7          | 69.6        | 88.3          | 58.4          | 56.0          |
| LP-Net [12]                             | 29.9        | 24.7          | <u>72.7</u>   | 46.8          | <u>49.6</u>   | 72.9        | 93.8          | 65.0          | 56.9          |
| ARL [9]                                 | 43.9        | 42.1          | 63.6          | 41.8          | 40.0          | <b>76.2</b> | <b>95.2</b>   | 66.8          | 58.7          |
| SRERL [20]                              | 45.7        | 47.8          | 59.6          | <u>47.1</u>   | 45.6          | 73.5        | 84.3          | 43.6          | 55.9          |
| JAAANet [10]                            | <b>62.4</b> | <u>60.7</u>   | 67.1          | 41.1          | 45.1          | 73.5        | 90.9          | <u>67.4</u>   | <u>63.5</u>   |
| <b>Ours</b>                             | [61.3]      | <b>[62.9]</b> | <b>[75.8]</b> | <b>[48.7]</b> | <b>[53.8]</b> | [75.5]      | [94.3]        | <b>[73.1]</b> | <b>[68.2]</b> |
| Pretrained on additional augmented data |             |               |               |               |               |             |               |               |               |
| UGN-B* [19]                             | 43.3        | 48.1          | 63.4          | 49.5          | 48.2          | 72.9        | 90.8          | 59.0          | 60.0          |
| HMP-PS* [31]                            | 21.8        | 48.5          | 53.6          | 56.0          | 58.7          | 57.4        | 55.9          | 56.9          | 61.0          |
| DML* [37]                               | 62.9        | 65.8          | 71.3          | 51.4          | 45.9          | 76.0        | 92.1          | 50.2          | 64.4          |
| <b>Ours</b>                             | [61.3]      | <u>[62.9]</u> | <b>[75.8]</b> | [48.7]        | <u>[53.8]</u> | [75.5]      | <b>[94.3]</b> | <b>[73.1]</b> | <b>[68.2]</b> |

TABLE III  
COMPARISONS OF AU RECOGNITION FOR 8 AUs ON DISFA IN TERMS OF ACCURACY AND AUC (IN %). \* MEANS THE METHOD EMPLOYED PRETRAINED MODEL ON ADDITIONAL DATASET.

| AU          | Accuracy |             |              |             |             | AUC       |            |             |             |
|-------------|----------|-------------|--------------|-------------|-------------|-----------|------------|-------------|-------------|
|             | JAA [15] | ARL [9]     | JAAANet [10] | UGN-B* [19] | <b>Ours</b> | DRML [38] | SRERL [20] | DML* [37]   | <b>Ours</b> |
| 1           | 93.4     | 92.1        | <b>97.0</b>  | 95.1        | [96.8]      | 53.3      | 76.2       | <b>90.5</b> | [89.5]      |
| 2           | 96.1     | 92.7        | <u>97.3</u>  | 93.2        | [97.4]      | 53.2      | 80.9       | <u>92.7</u> | [93.0]      |
| 4           | 86.9     | 88.5        | 88.0         | 88.5        | [92.7]      | 60.0      | 79.1       | <b>93.8</b> | [93.6]      |
| 6           | 91.4     | 91.6        | 92.1         | <b>93.2</b> | [92.1]      | 54.9      | 80.4       | <u>90.3</u> | [91.1]      |
| 9           | 95.8     | 95.9        | 95.6         | <u>96.8</u> | [96.9]      | 51.5      | 76.5       | <u>84.4</u> | [91.9]      |
| 12          | 91.2     | <b>93.9</b> | 92.3         | 93.4        | [93.4]      | 54.6      | 87.9       | <u>95.7</u> | [95.9]      |
| 25          | 93.4     | <b>97.3</b> | 94.9         | 94.8        | [96.8]      | 45.6      | 90.9       | <u>98.2</u> | [99.0]      |
| 26          | 93.2     | 94.3        | <u>94.8</u>  | 93.8        | [95.6]      | 45.3      | 73.4       | <u>87.4</u> | [94.4]      |
| <b>Avg.</b> | 92.7     | 93.3        | <u>94.0</u>  | 93.4        | [95.2]      | 52.3      | 80.7       | <u>91.6</u> | <b>93.6</b> |

where  $p_i$  and  $\hat{p}_i$  denote the ground-truth and predicted occurrence probability of  $i$ -th AU, respectively.  $w_i$  is the data balance weights, which is employed in [15]. Furthermore, we also minimize the loss of AU category classification  $\mathcal{L}_{int}$  by integrating all AUs information, including the refined AU features and the face alignment features, which is similar to the processing of  $\mathcal{L}_{au}$ .

We jointly integrate the face alignment and facial AU recognition into an end-to-end learning model. The face alignment loss is defined as:

$$\mathcal{L}_{align} = \frac{1}{2d_o^2} \sum_{i=1}^m [(x_i - \hat{x}_i)^2 + (y_i - \hat{y}_i)^2], \quad (11)$$

where  $(x_i, y_i)$  and  $(\hat{x}_i, \hat{y}_i)$  denote the ground-truth coordinate and corresponding predicted coordinate of the  $i$ -th facial landmark, and  $d_o$  is the ground-truth inter-ocular distance for

normalization [10]. Finally, the joint loss of our MGRR-Net is defined as:

$$\mathcal{L} = (\mathcal{L}_{au} + \mathcal{L}_{int}) + \lambda \mathcal{L}_{align}. \quad (12)$$

where  $\lambda$  is a tuning parameter for balancing.

## IV. EXPERIMENTS

### A. Dataset and Implementation Detail

**Dataset.** We provide evaluations on the popular BP4D [40] and DISFA [41] datasets. **BP4D** is a spontaneous facial AU database containing 328 facial videos from 41 participants (23 females and 18 males) who were involved in 8 sessions. Similar to [23], [9], [10], we consider 12 AUs and 140K valid frames with labels. **DISFA** consists of 27 participants (12 females and 15 males). Each participant has a video of 4,845 frames. We limited the number of AUs to 8 similar to [23], [10]. In comparison to BP4D, the experimental protocol and lighting conditions deliver DISFA to be a more challenging dataset. During training, each frame is annotated with 49 landmarks detected and calculated by SDM [42]. Following the experiment setting of [15], [10], we evaluated the model using the 3-fold subject-exclusive cross-validation protocol.

**Training strategy.** Our model is trained on a single NVIDIA RTX 2080Ti with 11 GB memory. The whole network is trained with the default initializer of PyTorch [43] with the SGD solver, a Nesterov momentum of 0.9 and a weight decay of 0.0005. The learning rate is set to 0.01 initially with a decay rate of 0.5 every 2 epochs. Maximum epoch number is set to 15. During training process, aligned faces are randomly cropped into  $176 \times 176$  and horizontally flipped. Regarding face alignment network and stem network, we set the value of the general parameters to be the same with [10]. The iteration layer number  $K$  is set to 2 except otherwise noted. The dimensionality of  $O_G$  is (64, 44, 44) and  $D$  is 1024. We employ  $L=8$  parallel attention layers in GATs. In our paper, all of the mapping Conv2D operations are used  $1 \times 1$  convolutional filters with a stride 1 and a padding 1. To reduce

TABLE IV  
COMPARISONS WITH STATE-OF-THE-ART METHODS FOR 12 AUs ON BP4D IN TERMS OF F1-FRAME, ACCURACY AND AUC RESPECTIVELY (IN %). \* MEANS THE METHOD EMPLOYED PRETRAINED MODEL ON ADDITIONAL DATASET, SO WE DO NOT COMPARE.

| AU   | F1-frame  |           |          |             |             |             |             |        |             |             |             |           |        |  |
|------|-----------|-----------|----------|-------------|-------------|-------------|-------------|--------|-------------|-------------|-------------|-----------|--------|--|
|      | MLCR [17] | DSIN [36] | JAA [15] | LP-Net [12] | ARL [9]     | SRERL[20]   | JAA-Net [9] | Ours   | R-CNN* [24] | UGN-B* [19] | HMP-PS*[31] | MDL*-[37] | Ours   |  |
| 1    | 42.4      | 51.7      | 47.2     | 43.3        | 45.8        | 46.9        | <b>53.8</b> | [52.6] | 50.2        | 54.2        | 53.1        | 52.6      | [52.6] |  |
| 2    | 36.9      | 40.4      | 44.0     | 38.0        | 39.8        | 45.3        | 47.8        | [47.9] | 43.7        | 46.4        | 46.1        | 44.9      | [47.9] |  |
| 4    | 48.1      | 56.0      | 54.9     | 54.2        | 55.1        | 55.6        | <b>58.2</b> | [57.3] | 57.0        | 56.8        | 56.0        | 56.2      | [57.3] |  |
| 6    | 77.5      | 76.1      | 77.5     | 77.1        | 75.7        | 77.1        | 78.5        | [78.5] | 78.5        | 76.2        | 76.5        | 79.8      | [78.5] |  |
| 7    | 77.6      | 73.5      | 74.6     | 76.7        | 77.2        | <b>78.4</b> | 75.8        | [77.6] | 78.5        | 76.7        | 76.9        | 80.4      | [77.6] |  |
| 10   | 83.6      | 79.9      | 84.0     | 83.8        | 82.3        | 83.5        | 82.7        | [84.9] | 82.6        | 82.4        | 82.1        | 85.2      | [84.9] |  |
| 12   | 85.8      | 85.4      | 86.5     | 87.2        | 86.6        | 87.6        | 88.2        | [88.4] | 87.0        | 86.1        | 86.4        | 88.3      | [88.4] |  |
| 14   | 61.0      | 62.7      | 61.9     | 63.6        | 58.8        | 63.9        | 63.7        | [67.8] | 67.7        | 64.7        | 64.8        | 65.6      | [67.8] |  |
| 15   | 43.7      | 37.3      | 43.6     | 45.3        | 47.6        | <b>52.2</b> | 43.3        | [47.6] | 49.1        | 51.2        | 51.5        | 51.7      | [47.6] |  |
| 17   | 63.2      | 62.9      | 60.3     | 60.5        | 62.1        | <b>63.9</b> | 61.8        | [63.3] | 62.4        | 63.1        | 63.0        | 59.4      | [63.3] |  |
| 23   | 42.1      | 38.8      | 42.7     | 48.1        | 47.4        | 47.1        | 45.6        | [47.4] | 50.4        | 48.5        | 49.9        | 47.3      | [47.4] |  |
| 24   | 55.6      | 41.6      | 41.9     | 54.2        | <b>55.4</b> | 53.3        | 49.9        | [51.3] | 49.3        | 53.6        | 54.5        | 49.2      | [51.3] |  |
| Avg. | 59.8      | 58.9      | 60.0     | 61.0        | 61.1        | 62.9        | 62.4        | [63.7] | 62.6        | 63.3        | 63.4        | 63.4      | [63.7] |  |

TABLE V  
COMPARISONS WITH STATE-OF-THE-ART METHODS FOR 12 AUs ON BP4D IN TERMS OF ACCURACY AND AUC RESPECTIVELY (IN %). \* MEANS THE METHOD EMPLOYED PRETRAINED MODEL ON ADDITIONAL DATASET, SUCH AS IMAGE-Net [39], *etc.* SO WE DO NOT DIRECTLY COMPARE.

| AU          | Accuracy    |             |             |              |               | AUC       |            |             |               |
|-------------|-------------|-------------|-------------|--------------|---------------|-----------|------------|-------------|---------------|
|             | UGN-B* [19] | JAA [15]    | ARL [9]     | JAA-Net [10] | Ours          | DRML [38] | SRERL [20] | DML* [37]   | Ours          |
| 1           | 78.6        | 74.7        | 73.9        | <u>75.2</u>  | <b>[78.7]</b> | 55.7      | 67.6       | <b>78.5</b> | [78.1]        |
| 2           | 80.2        | <u>80.8</u> | 76.7        | 80.2         | <b>[82.1]</b> | 54.5      | 70.0       | <u>75.9</u> | <b>[77.2]</b> |
| 4           | 80.0        | 80.4        | 80.9        | <b>82.9</b>  | [81.6]        | 58.8      | 73.4       | <b>84.4</b> | [83.8]        |
| 6           | 76.6        | 78.9        | 78.2        | <b>79.8</b>  | [78.7]        | 56.6      | 78.4       | <b>88.6</b> | [88.4]        |
| 7           | 72.3        | 71.0        | <b>74.4</b> | 72.3         | [73.7]        | 61.0      | 76.1       | <b>84.8</b> | [82.3]        |
| 10          | 77.8        | <u>80.2</u> | 79.1        | 78.2         | <b>[81.2]</b> | 53.6      | 80.0       | <b>87.3</b> | [86.3]        |
| 12          | 84.2        | 85.4        | 85.5        | <u>86.6</u>  | <b>[86.9]</b> | 60.8      | 85.9       | <b>93.9</b> | [93.6]        |
| 14          | 63.8        | 64.8        | 62.8        | <u>65.1</u>  | <b>[67.0]</b> | 57.0      | 64.4       | <u>71.8</u> | <b>[72.9]</b> |
| 15          | 84.0        | 83.1        | <u>84.7</u> | 81.0         | <b>[84.2]</b> | 56.2      | 75.1       | <u>80.7</u> | <b>[80.8]</b> |
| 17          | 72.8        | <u>73.5</u> | <b>74.1</b> | 72.8         | [72.2]        | 50.0      | 71.7       | <u>75.0</u> | <b>[78.2]</b> |
| 23          | 82.8        | 82.3        | 82.9        | 82.9         | <b>[84.1]</b> | 53.9      | 71.6       | <u>78.7</u> | <b>[79.3]</b> |
| 24          | 86.4        | 85.4        | 85.7        | <b>86.3</b>  | [86.0]        | 53.9      | 74.6       | <u>84.3</u> | <b>[87.8]</b> |
| <b>Avg.</b> | 78.2        | 78.4        | 78.2        | <u>78.6</u>  | <b>[79.7]</b> | 56.0      | 74.1       | <u>82.0</u> | <b>[82.4]</b> |

the parameters, we use a  $3 \times 3$  Conv2D operation with a stride 2 and a padding 1 before learning the channel-level feature.  $\lambda$  is empirically set to 0.5. Compared to JAA-Net [10], which takes 26.6ms per image to do a forward pass, our model takes just 16.5ms using an RTX 2080Ti GPU. This is due to the multi-head operation of the effective MH-GATs and the optimization of the model, which greatly reduce forward

pass time. In addition, we averaged the predicted probability of the local information and the integrated information as the final predicted activation probability for each AU, rather than simply using the integrated information of all the AUs.

**Evaluation metrics.** For all methods, the frame-based F1 score (F1-frame, %) is reported, which is the harmonic mean of the Precision P and Recall R and calculated by  $F1 = 2PR/(P + R)$ . To conduct a more comprehensive comparison with other methods, we also evaluate the performance with AUC (%) refers to the area under the ROC curve and accuracy (%). In addition, the average results over all AUs (denoted as **Avg.**) are computed with “%” omitted.

### B. Comparison with State-of-the-art Methods

We compare our proposed MGRR-Net with several frame-based AU detection baselines, including Deep Structure Inference Network (DSIN) [36], Joint AU Detection and Face Alignment (JAA) [15], Multi-Label Co-Regularization (MLCR) [17], Local relationship learning with Person-specific shape regularization (LP-Net) [12], Attention and Relation Learning (ARL) [9], Semantic Relationships Embedded Representation Learning (SRERL) [20], and Joint AU detection and face alignment via Adaptive Attention Network (JAA-Net) [10]. We directly use the results of these methods reported. Note that, the best and second best results are shown using bold and underline, respectively.

For a more comprehensive display, we also show methods (marked with \*) [44], [31], [19], [37] that use additional data, such as ImageNet [39] and VGGFace2 [45], *etc.*, for pre-training. From [12], [44], the pretrained feature extractor improved the average F1-score by at least 1.2% on BP4D dataset. Therefore, it is not fair to us to compare directly with them, because *we do not use any additional data* except the datasets



TABLE VI  
EFFECTIVENESS OF KEY COMPONENTS OF MGRR-NET EVALUATED ON DISFA IN TERMS OF F1-FRAME SCORE (IN %).

| Methods  | Setting |     |     |     | AU Index |        |        |        |        |        |        |        | Avg.   |
|----------|---------|-----|-----|-----|----------|--------|--------|--------|--------|--------|--------|--------|--------|
|          | D_G     | O_G | C_G | P_G | 1        | 2      | 4      | 6      | 9      | 12     | 25     | 26     |        |
| 1        |         |     |     |     | 47.1     | 61.1   | 66.3   | 44.7   | 52.2   | 74.9   | 92.2   | 66.2   | 63.1   |
| 2        | ✓       |     |     |     | 52.5     | 58.1   | 73.3   | 44.4   | 52.5   | 73.2   | 94.7   | 71.2   | 65.0   |
| 3        | ✓       | ✓   |     |     | 58.4     | 63.0   | 70.9   | 46.2   | 47.7   | 72.1   | 93.4   | 71.8   | 65.4   |
| 4        | ✓       |     | ✓   | ✓   | 60.0     | 65.7   | 67.4   | 43.8   | 57.1   | 75.4   | 93.3   | 64.7   | 65.9   |
| 5        | ✓       | ✓   | ✓   |     | 65.4     | 64.5   | 72.5   | 42.6   | 52.9   | 75.3   | 94.3   | 71.4   | 67.4   |
| 6        | ✓       | ✓   |     | ✓   | 61.0     | 67.3   | 76.8   | 40.9   | 58.0   | 74.8   | 93.7   | 65.8   | 67.3   |
| MGRR-Net | ✓       | ✓   | ✓   | ✓   | [61.3]   | [62.9] | [75.8] | [48.7] | [53.8] | [75.5] | [94.3] | [73.1] | [68.2] |

BP4D and DISFA. Due to the fact that our stem network only consists of a few simple convolutional layers, even if we pre-trained on additional datasets, it is unfair compared to pre-training on deeper feature extraction networks, such as ResNet50 [46]. In fact, our results are still excellent, which demonstrates the superiority and effectiveness of our proposed learning scheme. To provide a fair comparison, we omit the need for additional modal inputs and non-frame-based models [47], [48], [49], [50].

**Quantitative comparison on DISFA:** We compare our proposed method with its counterpart in Table II and Table III. It has been shown that our MGRR-Net outperforms all its competitors with impressive margins. Compared with the existing end-to-end feature learning and multi-label classification methods DSIN [36] and ARL [9], our MGRR-Net shows significant improvements on all AUs. J  ANet is the latest state of the art method which also joint AU detection and face alignment into an end-to-end multi-label multi-branch network. Compared with J  ANet [10], our MGRR-Net increases the average F1-frame and average accuracy by large margins of 4.7% and 1.2% and shows clear improvements for most annotated AU categories. The main reason lies in J  ANet completely ignores the correlation between branches and the individual modeling of each AU. Furthermore, we achieve the best performance in terms of average F1-frame, average accuracy and AUC, compared with all baselines.

**Quantitative comparison on BP4D:** AU detection results by different methods on BP4D are shown in Table IV and Table V, where the proposed MGRR-Net outperforms the state-of-the-art methods with impressive margins. Compared with the multi-branch combination-based J  ANet [10], the average F1 frame score and average accuracy score of MGRR-Net get 1.3% and 1.1% higher, respectively. Compared with the previous method DSIN [], which simultaneously modeled the deep feature learning and the structured AU relationship in an unified framework, our greatly outperforms it by 4.8% in terms of F1-frame. Furthermore, compared with latest graph-based relational modeling method SRERL [20], MGRR-Net increases the average F1-frame and average AUC by large margins of 0.8% and 8.3%. This is mainly due to the fact that the proposed method models the semantic relationships among AUs while also gaining complementary features from multiple global perspectives to increase the distinguishability of each AU. In addition, MGRR-Net achieves the best or second-best

detection performance for most of the 12 AUs annotated in BP4D compared with the state-of-the-art methods. And compared with the advanced models pre-trained with additional data (marked with \* in Table IV and Table V), our MGRR-Net still has strong competitiveness.

Experimental results of MGRR-Net demonstrate its effectiveness in improving AU detection accuracy on DISFA and BP4D, as well as good robustness and generalization ability.

### C. Ablation Studies

We perform detailed ablation studies on DISFA to investigate the effectiveness of each part of our proposed MGRR-Net. Due to space limitations, we do not show the ablation results for BP4D, but it is consistent with DISFA. To assess the effect of different components, we run the experiments with same parameter setting (e.g. layer K=2) for variations of the proposed network in Table VI.

1) *Effects of region-level dynamic graph (D\_G):* In Table VI, we can see that learning by the dynamic graph initialized with prior knowledge outperforms baseline with an improvement of average F1-frame from 63.1% to 65.0%, indicating that the dynamic graph could get richer features from other correlated AU regions to improve robustness. Furthermore, to cancel out the initialization of prior knowledge, we randomly initialize the dynamic graph, which decreases F1-frame to 64.7%. These observations suggest that the relationship reasoning in the dynamic graph can significantly boost the performance of AU detection, while prior knowledge makes a great contribution but not predominantly.

2) *Effects of multi-level global features:* We test the contributions of multiple important global feature components of the model in Table VI, namely, original global feature (O\_G) from stem network, channel-level global feature (C\_G) from channel-level MH-GAT and pixel-level global feature (P\_G) from pixel-level MH-GAT. After we supplemented original global feature (O\_G) for each target AU, the average F1-frame score has been improved from 65.0% to 65.4%, demonstrating the effectiveness of global detail supplementation. The fusion of channel- and pixel-level global features (C\_G and P\_G) results in a 0.9% increase, indicating that they make the AU more discriminative than only using the original global features. Comparing the results of the fifth test (with C\_G) and the sixth test (with P\_G) in Table VI with the third test, one of the channel-level and pixel-level global features can boost the

TABLE VII  
PERFORMANCE COMPARISON OF MGRR-NET WITH DIFFERENT  
ITERATION STEP NUMBER K ON DISFA IN TERMS OF F1-FRAME SCORE  
(IN %).

| Layers | AU Index    |             |             |             |             |             |             |             | Avg.        |
|--------|-------------|-------------|-------------|-------------|-------------|-------------|-------------|-------------|-------------|
|        | 1           | 2           | 4           | 6           | 9           | 12          | 25          | 26          |             |
| K=1    | 64.5        | 58.3        | 74.9        | 46.1        | <b>54.4</b> | 75.4        | 92.3        | 73.1        | 67.4        |
| K=2    | 61.3        | 62.9        | 75.8        | <b>48.7</b> | 53.8        | <b>75.5</b> | <b>94.3</b> | <b>73.1</b> | <b>68.2</b> |
| K=3    | <b>65.5</b> | <b>67.0</b> | <b>77.6</b> | 40.0        | 44.9        | 75.1        | 94.0        | 68.8        | 66.6        |

TABLE VIII  
MEAN ERROR (%) RESULTS OF DIFFERENT FACE ALIGNMENT MODELS ON  
DISFA AND BP4D (LOWER IS BETTER).

| Datasets | MCL  | JAA  | JAA <sup>Net</sup> | Ours        |
|----------|------|------|--------------------|-------------|
| DISFA    | 7.15 | 6.30 | 4.02               | <b>3.95</b> |
| BP4D     | 7.20 | 6.38 | <b>3.80</b>        | 4.01        |

performance by roughly the same amount. It suggests that by supplementing and training different levels of global features for each AU branch, more global details can be provided to detect AUs in terms of different expressions and individuals.

Finally, the hierarchical gated fusion of multi-level global and local features leads to a significant performance improvement to 68.2% in terms of F1-frame score. It validates that the dynamic relationship of multiple related face regions provides more robustness, while the supplementation of multi-level global features makes the AU more discriminative.

3) *Effects of layer number.*: We evaluate the impact of layer number of our proposed iterative reasoning network. As shown in Table VII, MGRR-Net achieves the averaged F1-frame score of 67.4%, 68.2% and 66.6% on DISFA when the reasoning layer number K is set to 1, 2 and 3 respectively. And the averaged F1-frame scores on BP4D are 63.5%, 63.7%, and 63.1% respectively, which are not shown in detail due to space limitation. The optimal number of layers is 2 for our MGRR-Net on DISFA and BP4D datasets.

4) *Results for face alignment.*: We jointly take face alignment network into our MGRR-Net via auxiliary training, which can provide effective muscle regions corresponding to AUs based on the detected landmarks. Table VIII shows the mean error results of our MGRR-Net and baseline method JAA<sup>Net</sup> [10] on DISFA and BP4D. We also compare with state-of-the-art face alignment methods that have released trained models, including MCL [51], JAA [15]. Our MGRR-Net achieves competitive 3.95 and 4.01 mean error on DISFA and BP4D respectively. It indicates that with the comparable face alignment performance as JAA<sup>Net</sup>, our MGRR-Net can achieve better AU detection accuracy.

#### D. Visualization of Results

To better understand the effectiveness of our proposed model, we visualize the learned class activation maps of MGRR-Net corresponding to different AUs in terms of different expressions, postures and individuals, as shown in Fig. 3. Two examples are from DISFA and two are from BP4D, containing visualization results of different genders

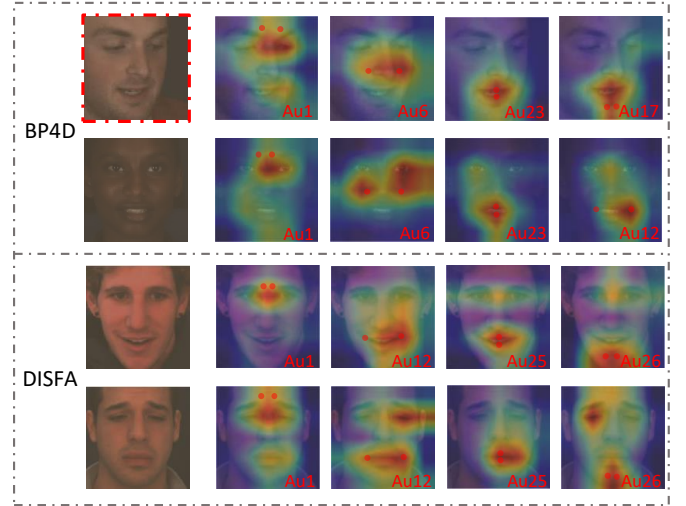


Fig. 3. Class activation maps that show the discriminative regions for different AUs in terms of different expressions and individuals on DISFA and BP4D datasets.

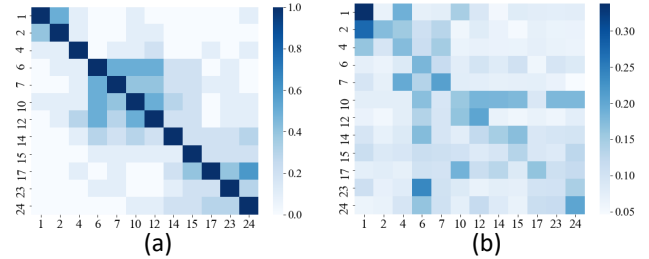


Fig. 4. Visualizations of the predefined AU correlation (a) and the learned relevance matrix (b) for the individual (marked with red box) on BP4D in the first row of Figure 3.

and different poses with different AU categories. Through the learning of MGRR-Net, not only the concerned AU regions can be accurately located, but also the positive correlation with other AU areas can be established and other details of the global face can be supplemented. The different activation maps of the same AU on different individuals show that our MGRR-Net can dynamically adjust according to the differences of expression, posture, and individual. In addition, as shown in Fig. 4, we further visualize the learned relevance matrix (marked as (b)) and the predefined AU correlations (marked as (a)) of the individual (marked with red box) corresponding to the first row of Fig. 3 on BP4D. The predefined correlation matrices are used to roughly calculate the co-occurrence relevance between different AUs by counting the dependence of positive and negative samples. It over-emphasise target AU as well as a few other AUs while other AU regions are completely ignored, due to bias in the statistics of the data. From the correlation matrix we learned, the target AU and the relevant AU are highlighted without discarding information from other branches at all, which is beneficial for increasing the distinguishability between AUs. Furthermore, the supplementation of global features with multiple perspectives allows different AUs to access a lot of information outside the defined areas, as shown in Fig. 3, which is helpful for adaptive changes in



terms of different individuals and their expressions.

## V. CONCLUSION

In this paper, we have proposed a novel multi-level graph relational reasoning network (termed MGRR-Net) for facial AU detection. Each layer of MGRR-Net can encode the dynamic relationships among AUs via a region-level relationship graph and complementary multiple levels of global information covering expression and subject diversities. The multi-layer iterative feature refinement finally obtains robust and discriminative features for each AU. Extensive experimental evaluations on DISFA and BP4D show that our MGRR-Net outperforms state-of-the-art AU detection methods with impressive margins.

In our future work, we would like to investigate the further implementation of facial AU detection into real applications, such as automatically estimating facial Palsy severeness for patients. This will improve the well-being of people suffering from facial palsy across the world. In collaboration with medical professionals, we will collect and annotate facial palsy datasets such as [52], to further validate the migration capability and effectiveness of the proposed model.

## REFERENCES

- [1] P. Ekman and E. L. Rosenberg, *What the face reveals: Basic and applied studies of spontaneous expression using the Facial Action Coding System (FACS)*. Oxford University Press, USA, 1997.
- [2] M. Dahmane and J. Meunier, "Prototype-based modeling for facial expression analysis," *IEEE Transactions on Multimedia*, vol. 16, no. 6, pp. 1574–1584, 2014.
- [3] H. Li, J. Sun, Z. Xu, and L. Chen, "Multimodal 2d+ 3d facial expression recognition with deep fusion convolutional neural network," *IEEE Transactions on Multimedia*, vol. 19, no. 12, pp. 2816–2831, 2017.
- [4] D. R. Rubinow and R. M. Post, "Impaired recognition of affect in facial expression in depressed patients," *Biological Psychiatry*, vol. 31, no. 9, pp. 947–953, 1992.
- [5] X. Niu, H. Han, J. Zeng, X. Sun, S. Shan, Y. Huang, S. Yang, and X. Chen, "Automatic engagement prediction with gap feature," in *Proceedings of the 20th ACM International Conference on Multimodal Interaction*, 2018, pp. 599–603.
- [6] R. S. Feldman, L. Jenkins, and O. Popoola, "Detection of deception in adults and children via facial expressions," *Child Development*, pp. 350–355, 1979.
- [7] Y. Tong and Q. Ji, "Learning bayesian networks with qualitative constraints," in *Proceedings of the IEEE conference on computer vision and pattern recognition*, 2008, pp. 1–8.
- [8] Y. Li, S. Wang, Y. Zhao, and Q. Ji, "Simultaneous facial feature tracking and facial expression recognition," *IEEE Transactions on image processing*, vol. 22, no. 7, pp. 2559–2573, 2013.
- [9] Z. Shao, Z. Liu, J. Cai, Y. Wu, and L. Ma, "Facial action unit detection using attention and relation learning," *IEEE transactions on affective computing*, 2019.
- [10] Z. Shao, Z. Liu, J. Cai, and L. Ma, "Jaa-net: joint facial action unit detection and face alignment via adaptive attention," *International Journal of Computer Vision*, vol. 129, no. 2, pp. 321–340, 2021.
- [11] P. Liu, J. T. Zhou, I. W.-H. Tsang, Z. Meng, S. Han, and Y. Tong, "Feature disentangling machine-a novel approach of feature selection and disentangling in facial expression analysis," in *Proceedings of the European Conference on Computer Vision*, 2014, pp. 151–166.
- [12] X. Niu, H. Han, S. Yang, Y. Huang, and S. Shan, "Local relationship learning with person-specific shape regularization for facial action unit detection," in *Proceedings of the IEEE Conference on Computer Vision and Pattern Recognition*, 2019, pp. 11 917–11 926.
- [13] S. Hochreiter and J. Schmidhuber, "Long short-term memory," *Neural Computation*, vol. 9, no. 8, pp. 1735–1780, 1997.
- [14] K. Zhao, W.-S. Chu, F. De la Torre, J. F. Cohn, and H. Zhang, "Joint patch and multi-label learning for facial action unit and holistic expression recognition," *IEEE Transactions on Image Processing*, vol. 25, no. 8, pp. 3931–3946, 2016.
- [15] Z. Shao, Z. Liu, J. Cai, and L. Ma, "Deep adaptive attention for joint facial action unit detection and face alignment," in *Proceedings of the European Conference on Computer Vision*, 2018, pp. 705–720.
- [16] Y. Zhang, W. Dong, B.-G. Hu, and Q. Ji, "Classifier learning with prior probabilities for facial action unit recognition," in *Proceedings of the IEEE conference on computer vision and pattern recognition*, 2018, pp. 5108–5116.
- [17] X. Niu, H. Han, S. Shan, and X. Chen, "Multi-label co-regularization for semi-supervised facial action unit recognition," in *Advances in Neural Information Processing Systems*, 2019, pp. 909–919.
- [18] Z. Liu, J. Dong, C. Zhang, L. Wang, and J. Dang, "Relation modeling with graph convolutional networks for facial action unit detection," in *International Conference on Multimedia Modeling*. Springer, 2020, pp. 489–501.
- [19] T. Song, L. Chen, W. Zheng, and Q. Ji, "Uncertain graph neural networks for facial action unit detection," in *Proceedings of the AAAI Conference on Artificial Intelligence*, 2021, p. 5993–6001.
- [20] G. Li, X. Zhu, Y. Zeng, Q. Wang, and L. Lin, "Semantic relationships guided representation learning for facial action unit recognition," in *Proceedings of the AAAI Conference on Artificial Intelligence*, 2019, pp. 8594–8601.
- [21] P. Veličković, G. Cucurull, A. Casanova, A. Romero, P. Liò, and Y. Bengio, "Graph attention networks," in *International Conference on Learning Representations*, 2018, pp. 1–12.
- [22] L. Zhong, Q. Liu, P. Yang, J. Huang, and D. N. Metaxas, "Learning multiscale active facial patches for expression analysis," *IEEE transactions on cybernetics*, vol. 45, no. 8, pp. 1499–1510, 2014.
- [23] W. Li, F. Abtahi, and Z. Zhu, "Action unit detection with region adaptation, multi-labeling learning and optimal temporal fusing," in *Proceedings of the IEEE Conference on Computer Vision and Pattern Recognition*, 2017, pp. 1841–1850.
- [24] C. Ma, L. Chen, and J. Yong, "Au r-cnn: Encoding expert prior knowledge into r-cnn for action unit detection," *neurocomputing*, vol. 355, pp. 35–47, 2019.
- [25] S. Taheri, Q. Qiu, and R. Chellappa, "Structure-preserving sparse decomposition for facial expression analysis," *IEEE Transactions on Image Processing*, vol. 23, no. 8, pp. 3590–3603, 2014.
- [26] K. Zhao, W.-S. Chu, F. De la Torre, J. F. Cohn, and H. Zhang, "Joint patch and multi-label learning for facial action unit detection," in *Proceedings of the IEEE Conference on Computer Vision and Pattern Recognition*, 2015, pp. 2207–2216.
- [27] S. Jaiswal and M. Valstar, "Deep learning the dynamic appearance and shape of facial action units," in *IEEE Winter Conference on Applications of Computer Vision*, 2016, pp. 1–8.
- [28] A. Graves and J. Schmidhuber, "Framewise phoneme classification with bidirectional lstm and other neural network architectures," *Neural Networks*, vol. 18, no. 5-6, pp. 602–610, 2005.
- [29] W. Li, F. Abtahi, Z. Zhu, and L. Yin, "Eac-net: Deep nets with enhancing and cropping for facial action unit detection," *IEEE Transactions on Pattern Analysis and Machine Intelligence*, vol. 40, no. 11, pp. 2583–2596, 2018.
- [30] X. Ge, P. Wan, H. Han, J. M. Jose, Z. Ji, Z. Wu, and X. Liu, "Local global relational network for facial action units recognition," in *IEEE International Conference on Automatic Face and Gesture Recognition*. IEEE, 2021, pp. 01–08.
- [31] T. Song, Z. Cui, W. Zheng, and Q. Ji, "Hybrid message passing with performance-driven structures for facial action unit detection," in *Proceedings of the IEEE/CVF Conference on Computer Vision and Pattern Recognition*, 2021, pp. 6267–6276.
- [32] S. Yan, Y. Xiong, and D. Lin, "Spatial temporal graph convolutional networks for skeleton-based action recognition," in *Thirty-second AAAI conference on artificial intelligence*, 2018.
- [33] Z. Wang, T. Chen, J. Ren, W. Yu, H. Cheng, and L. Lin, "Deep reasoning with knowledge graph for social relationship understanding," *arXiv preprint arXiv:1807.00504*, 2018.
- [34] X. Liang, X. Shen, J. Feng, L. Lin, and S. Yan, "Semantic object parsing with graph lstm," in *European Conference on Computer Vision*. Springer, 2016, pp. 125–143.
- [35] A. Vaswani, N. Shazeer, N. Parmar, J. Uszkoreit, L. Jones, A. N. Gomez, E. Kaiser, and I. Polosukhin, "Attention is all you need," *Advances in neural information processing systems*, vol. 30, 2017.
- [36] C. Corneanu, M. Madadi, and S. Escalera, "Deep structure inference network for facial action unit recognition," in *Proceedings of the European Conference on Computer Vision*, 2018, pp. 298–313.
- [37] S. Wang, Y. Chang, and C. Wang, "Dual learning for joint facial landmark detection and action unit recognition," *IEEE Transactions on Affective Computing*, 2021.

- [38] K. Zhao, W.-S. Chu, and H. Zhang, "Deep region and multi-label learning for facial action unit detection," in *Proceedings of the IEEE conference on computer vision and pattern recognition*, 2016, pp. 3391–3399.
- [39] J. Deng, W. Dong, R. Socher, L.-J. Li, K. Li, and L. Fei-Fei, "Imagenet: A large-scale hierarchical image database," in *Proceedings of the IEEE conference on computer vision and pattern recognition*, 2009, pp. 248–255.
- [40] X. Zhang, L. Yin, J. F. Cohn, S. Canavan, M. Reale, A. Horowitz, P. Liu, and J. M. Girard, "Bp4d-spontaneous: a high-resolution spontaneous 3d dynamic facial expression database," *Image and Vision Computing*, vol. 32, no. 10, pp. 692–706, 2014.
- [41] S. M. Mavadati, M. H. Mahoor, K. Bartlett, P. Trinh, and J. F. Cohn, "Disfa: A spontaneous facial action intensity database," *IEEE Transactions on Affective Computing*, vol. 4, no. 2, pp. 151–160, 2013.
- [42] X. Xiong and F. De la Torre, "Supervised descent method and its applications to face alignment," in *Proceedings of the IEEE conference on computer vision and pattern recognition*, 2013, pp. 532–539.
- [43] A. Paszke, S. Gross, F. Massa, A. Lerer, J. Bradbury, G. Chanan, T. Killeen, Z. Lin, N. Gimelshein, L. Antiga *et al.*, "Pytorch: An imperative style, high-performance deep learning library," in *Advances in neural information processing systems*, 2019, pp. 8026–8037.
- [44] G. M. Jacob and B. Stenger, "Facial action unit detection with transformers," in *Proceedings of the IEEE/CVF Conference on Computer Vision and Pattern Recognition*, 2021, pp. 7680–7689.
- [45] Q. Cao, L. Shen, W. Xie, O. M. Parkhi, and A. Zisserman, "Vggface2: A dataset for recognising faces across pose and age," in *13th IEEE international conference on automatic face & gesture recognition*, 2018, pp. 67–74.
- [46] K. He, X. Zhang, S. Ren, and J. Sun, "Deep residual learning for image recognition," in *Proceedings of the IEEE conference on computer vision and pattern recognition*, 2016, pp. 770–778.
- [47] P. Liu, Z. Zhang, H. Yang, and L. Yin, "Multi-modality empowered network for facial action unit detection," in *IEEE Winter Conference on Applications of Computer Vision*, 2019, pp. 2175–2184.
- [48] H. Yang, T. Wang, and L. Yin, "Adaptive multimodal fusion for facial action units recognition," in *Proceedings of the 28th ACM International Conference on Multimedia*, 2020, pp. 2982–2990.
- [49] Z. Shao, L. Zou, J. Cai, Y. Wu, and L. Ma, "Spatio-temporal relation and attention learning for facial action unit detection," *arXiv preprint arXiv:2001.01168*, 2020.
- [50] H. Yang, L. Yin, Y. Zhou, and J. Gu, "Exploiting semantic embedding and visual feature for facial action unit detection," in *Proceedings of the IEEE/CVF Conference on Computer Vision and Pattern Recognition*, 2021, pp. 10482–10491.
- [51] Z. Shao, H. Zhu, X. Tan, Y. Hao, and L. Ma, "Deep multi-center learning for face alignment," *Neurocomputing*, vol. 396, pp. 477–486, 2020.
- [52] B. F. O'Reilly, J. J. Soraghan, S. McGrenary, and S. He, "Objective method of assessing and presenting the house-brackmann and regional grades of facial palsy by production of a facogram," *Otology & Neurotology*, vol. 31, no. 3, pp. 486–491, 2010.



**Xuri Ge** received the M.S. degree in computer science from the School of Information Science and Engineering, Xiamen University, China, in 2020. He is currently pursuing the Ph.D. degree with the school of computer science, University of Glasgow, Scotland, UK. His current research interests include computer vision, medical image processing, and multimedia processing.



**Joemon M. Jose** is a Professor at the School of Computing Science, University of Glasgow, Scotland and a member of the Information Retrieval group. His research focuses around the following three themes: (i) Social Media Analytics; (ii) Multi-modal interaction for information retrieval; (iii) Multimedia mining and search. He has published over 300 papers with more than 8000 Google Scholar citations, and an h-index of 47. He leads the Multimedia Information Retrieval group which investigates research issues related to the above themes.



**Songpei Xu** received the M.S. degree in data science from the school of computer science, University of Glasgow, Scotland, UK. She is currently pursuing the Ph.D. degree with the school of computer science, University of Glasgow, Scotland, UK. Her current research interests include machine learning, pattern recognition and Human-computer interaction.



**Xiao Liu** received the Ph.D. degree in computer science from Zhejiang University in 2015. He worked at Baidu from 2015 to 2019 and at Tomorrow Advancing Life Education Group (TAL) from 2019 to 2021. He is currently a Researcher with the Online Media Business Unit at Tencent, Beijing, China. His research interests include the applied AI, such as intelligent multimedia processing, computer vision, and learning systems. His research results have expounded in more than 40 publications at journals and conferences, such as IEEE TRANSACTIONS ON IMAGE PROCESSING, IEEE TRANSACTIONS ON NEURAL NETWORKS AND LEARNING SYSTEMS, CVPR, ICCV, ECCV, AAAI, and MM. As a Key Team Member, he achieved the best performance in various competitions, such as the ActivityNet challenges, NTIRE super resolution challenge, and EmotionNet facial expression recognition challenge.



**Hu Han** (Member, IEEE) received the Ph.D. degree in computer science from the Institute of Computing Technology (ICT), Chinese Academy of Sciences (CAS), Beijing, China, in 2011. He was a Research Associate with the Pattern Recognition and Image Processing (PRIP) Laboratory, Michigan State University, East Lansing, MI, USA, and a Visiting Researcher with Google, Mountain View, CA, USA, from 2011 to 2015. He is currently an Associate Professor with ICT, CAS. He has published more than 70 papers in journals and conference, including IEEE TRANSACTIONS ON PATTERN ANALYSIS AND MACHINE INTELLIGENCE, IEEE TRANSACTIONS ON IMAGE PROCESSING, IEEE TRANSACTIONS ON INFORMATION FORENSICS AND SECURITY, IEEE TRANSACTIONS ON BIOMETRICS, BEHAVIOR, AND IDENTITY SCIENCE, Pattern Recognition, CVPR, NeurIPS, ECCV, and MICCAI, with more than 4000 Google Scholar citations. His research interests include computer vision, pattern recognition, and biometrics. He was a recipient of the 2020 IEEE Signal Processing Society Best Paper Award, the 2019 IEEE FG Best Poster Presentation Award, and the 2016/2018 CCBP Best Student/Poster Award. He is/was an Associate Editor of Pattern Recognition, the Area Chair of ICPR2020, and a Senior Program Committee Member of IJCAI2021.